Current Applied Physics 12 (2012) 849–853

Contents lists available at SciVerse ScienceDirect

Current Applied Physics

journal homepage: www.elsevier.com/locate/cap

# Structural and nanomechanical properties of *a*-plane ZnO thin films deposited under different oxygen partial pressures

Sheng-Rui Jian [a,*], Hou-Guang Chen [a], Guo-Ju Chen [a], Jason S.C. Jang [b], Jenh-Yih Juang [c]

[a] Department of Materials Science and Engineering, I-Shou University, Kaohsiung 840, Taiwan, ROC
[b] Institute of Materials Science and Engineering, Department of Mechanical Engineering, National Central University, Chung-Li 320, Taiwan, ROC
[c] Department of Electrophysics, National Chiao Tung University, Hsinchu 300, Taiwan, ROC

ARTICLE INFO

*Article history:*
Received 28 August 2011
Received in revised form
15 October 2011
Accepted 14 November 2011
Available online 20 November 2011

*Keywords:*
*a*-Plane ZnO thin film
Nanoindentation
Focused ion beam
Cross-sectional transmission electron microscopy

ABSTRACT

The effects of $O_2$ partial pressure during RF magnetron sputtering on the structural and nanomechanical properties of *a*-plane ZnO thin films were investigated by using X-ray diffraction (XRD) and nanoindentation techniques. The XRD and the transmission electron microscopy (TEM) selected area diffraction results indicate that the epitaxial relationship between ZnO thin films and $Al_2O_3$ substrates is ZnO $(11\bar{2}0)//Al_2O_3$ $(1\bar{1}02)$. The average values of the hardness and Young's modulus of the *a*-plane ZnO films were found to decrease with increasing oxygen partial pressure. The cross-sectional TEM revealing the localized plastic deformation of ZnO thin films beneath the Berkovich indenter, indicating the prominent role played by the threading dislocations in the film deformation behavior. At higher indentation loadings, the sapphire substrate exhibits extensive deformation with narrow slip bands appearing on {0001} plane. However, no evidence of pressure-induced phase transformation, as well as cracking and/or delamination phenomena at the film–substrate interface was observed.



## 1. Introduction

ZnO has attracted extensive attention because of the tremendous application potential promised by its large direct band gap of 3.37 eV, high exciton binding energy of 60 meV, high transparency, piezoelectricity, and even room-temperature ferromagnetism [1–4]. However, similar to those encountered with the *c*-plane GaN, the *c*-plane ZnO commonly used in fabricating quantum well as well as the heterostructure-based optoelectronic devices have been found to suffer from undesirable spontaneous and piezoelectric polarizations in the active layer which may lowers the quantum efficiency drastically [5]. In this respect, the use of non-polar *a*-plane ZnO and *m*-plane ZnO which have equal number of cations and anions on the surface seems to offer a plausible alternative. Non-polar ZnO surfaces also have in-plane structural, optical, acoustic and electrical anisotropic characteristics that might be useful for novel device applications, such as the UV modulators [6]. However, it has been pointed out that, in single crystalline ZnO, the hardness is the smallest when probed normal to the *a*-plane [7]. Since for most device fabrication processes contact-induced damage may significantly affect the ultimate optical and electronic properties of the device, thus a quantitative assessment of the material's mechanical properties is of crucial importance. In particular, with the smaller hardness and Young's modulus inherent to ZnO, as compared to that of GaN, the reliability issues concerning delamination, brittle fracture, and fatigue degradation of the thin film structures could become major concerns in device manufacturing.

Nanoindentation has been widely used for characterizing the mechanical properties of various nanomaterials [8,9] and thin films [10–12], due to its high sensitivity, good resolution and easy operation. Among the mechanical properties of interest, hardness, Young's modulus and elastic/plastic deformation behavior are readily obtained from nanoindentation testing. For preparing ZnO in thin film form, several techniques, such as magnetron sputtering [13], pulsed laser deposition [14], metal-organic chemical vapor deposition [15], and molecular beam epitaxy [16] have been extensively developed. Among them, magnetron sputtering operated with oxygen and argon mixture has been widely used for fabricating uniform large area ZnO thin films at relatively lower temperatures. We note that, although the prominent roles played by oxygen in determining the electro-optical properties of the obtained ZnO films, investigations to correlate the partial pressure of oxygen in the sputtering gas mixture with the structural and mechanical characteristics of the *a*-plane ZnO thin films deposited on the *r*-plane sapphire substrates by RF magnetron sputtering are, nevertheless, still lacking.

* Corresponding author. Tel.: +886 7 6577711x3130; fax: +886 7 6578444.
*E-mail address:* srjian@gmail.com (S.-R. Jian).

1567-1739/$ – see front matter © 2011 Elsevier B.V. All rights reserved.
doi:10.1016/j.cap.2011.11.018

The aim of this study is to investigate the nanomechanical characterizations of the *a*-plane ZnO thin films deposited by RF sputtering at various $O_2$/Ar ratios. Changes in mechanical properties for films obtained under the systematically varied $O_2$/Ar ratio are discussed in conjunction with the resultant film crystallinity and grain size. Furthermore, by combining the load–displacement data with the nanoindentation-induced deformation structures using scanning electron microscopy (SEM) and cross-sectional transmission electron microscopy (XTEM), important aspects of the contact-induced deformation mechanisms prevailing in these *a*-plane ZnO thin films are revealed.

## 2. Experimental details

For growing the *a*-plane-oriented ZnO films with RF-sputtering system, the $(1\bar{1}02)$ -oriented (*r*-plane) sapphire substrates were used. Prior to depositing the ZnO thin films, the as-received *r*-plane sapphire substrates with typical size of $1 \times 1$ cm$^2$ were annealed at 1200 °C for 1 h followed by acetone cleaning. Sintered ZnO ceramic disks were used as the sputtering targets. For the sputtering process, the vacuum chamber was first evacuated to a base pressure of $10^{-6}$ Torr, and then gas mixture of Ar and $O_2$ was introduced into the chamber with a constant pressure of 5 mTorr. The ratio of $O_2$ gas was varied from 20% to 80% of the total sputtering gas. All ZnO films were deposited at ambient temperature with an input power of 100 W for 30 min. The thickness of the resultant ZnO films is about 200 nm.

The crystal structure of *a*-plane ZnO thin films was analyzed by X-ray diffractometer (Panalytical X'Pert XRD). The hardness and the elastic modulus of the *a*-plane ZnO thin films were calculated from the load–displacement ($P$–$h$) data obtained by nanoindentation using a TroboScope nanomechanical testing systems (Hysitron Inc.). The Hysitron nanoindenter monitors and records the load and displacement of a Berkovich three-sided diamond pyramid indenter with a force resolution of about 1 nN and displacement resolution of about 0.1 nm. All nanoindentation measurements were performed with the thermal drift being smaller than 0.01 nm/s. The thermal drift effects were corrected for each test using a holding segment in air prior to indentation. The indentation impressions were imaged *in situ* using the same indenter tip. At least 10 indentations were made on each specimen and the values of hardness and Young's modulus of thin films were determined by taking the average results obtained from each indentation. The indentations were separated by more than 50 μm to avoid mutual interactions. A typical indentation experiment consists of four sequential steps: (1) approaching the indenter to surface; (2) loading to the peak load at a loading rate of 10 μN/s; (3) holding the indenter at the peak load for 5 s; and (4) unloading completely. The holding step was included to avoid the influence of creep on the unloading characteristics since the unloading curve was used to obtain the elastic modulus of a material.

Nanoindentation hardness is defined as the indentation load divided by the projected contact area of the indentation. It is the mean pressure received by the material under loading. Therefore, at the peak load $P_{max}$, the hardness $H$ of the material under test can be obtained by the following expression:

$$H = \frac{P_{max}}{A}, \tag{1}$$

where $A$ is the projected contact area. For an indenter with known geometry, such as the Berkovich indenter tip used in this work, the projected contact area is a function of contact depth, which is measured by the nanoindenter *insitu* during indentation [17].

The elastic modulus was calculated using the Oliver–Pharr analysis procedure [18] beginning by fitting the unloading curve to a power–law relation. The unloading stiffness can be obtained from the slope of the initial portion of the unloading curves, $S = dP/dh$. Based on the relationships developed by Sneddon [19] for the indentation of an elastic half space by any punch that can be described as a solid of revolution of a smooth function, a geometry independent relation involving contact stiffness, contact area and elastic modulus can be derived as:

$$S = 2\beta E_r \sqrt{\frac{A}{\pi}}, \tag{2}$$

where $\beta$ is a constant which depends on the geometry of the indenter ($\beta$ is 1.034 for Berkovich indenter) [17], and $E_r$ is the reduced elastic modulus which accounts for the fact that elastic deformation occurs in both the sample and indenter. Thus, $E_r$ is given by:

$$\frac{1}{E_r} = \frac{1-\nu_f^2}{E_f} + \frac{1-\nu_i^2}{E_i}, \tag{3}$$

where $E_f$ and $\nu_f$ respectively denote the elastic modulus and Poisson's ratio of the thin films and, $E_i$ and $\nu_i$ are the corresponding quantities for the indenter. For diamond indenter tip, $E_i = 1141$ GPa, $\nu_i = 0.07$ and, $\nu_f = 0.25$ is chosen for ZnO thin films [14].

Moreover, in order to reveal the deformation behavior displayed in the indentation measurement, cyclic nanoindentation tests were also performed with a Nanoindenter XP instrument system [20,21] (MTS Cooperation, Nano Instruments Innovation Center, TN, USA). After being indented to a maximum load of 80 mN, samples for XTEM examinations were prepared from regions within the indents by means of the dual-beam focused ion beam (FIB, Nova 220) station with 30 keV Ga ions. Prior to milling, the FIB was used to deposit a Pt layer of ~1 μm thick to protect the sample surface. Fig. 1 displays a typical scanning electron microscopy (SEM) image of the sample at the final stage of FIB milling procedures. The details of FIB produces in preparing XTEM sample can be found elsewhere

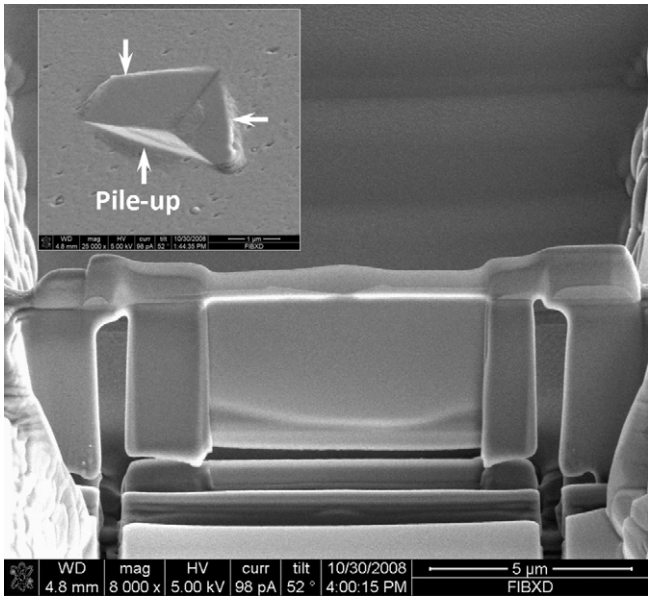


**Fig. 1.** Illustration of final procedure for FIB milling sample preparation. The sample can be plucked by a shape glass tip under an optical microscopy outside FIB station. Inset: SEM micrograph of an indent at indentation load of 80 mN. The pile-up event around the indented area is observed.

[22]. The XTEM lamellas were examined in a FEI TECNAI $G^2$ TEM operated at 200 kV.

## 3. Results and discussion

Fig. 2 shows the XRD results of ZnO thin films obtained by using sputtering gases with different $O_2$/Ar ratios. It is evident that, in addition to the $(1\bar{1}02)$ and $(2\bar{2}04)$ diffraction peaks from the sapphire substrate, there is also a diffraction peak locating at $2\theta = 56.6^\circ$ indicating the growth of $(11\bar{2}0)$ -oriented *a*-plane ZnO films in each case. In addition, there is no evidence for the existence of the ZnO (0002) reflection ($2\theta = 34.4^\circ$), indicating that the obtained ZnO films are all non-polar *a*-plane ZnO thin films and the epitaxial relationship between film and substrate is $(1\bar{1}02)$ $Al_2O_3$// $(11\bar{2}0)$ ZnO. It is also noted that the intensity of the $(11\bar{2}0)$ peak appears to grow with increasing $O_2$/Ar ratio, while the peak full-width-at-half-maximum (FWHM) becomes narrower when the $O_2$/Ar ratio increases. Since both film crystallinity and grain size are the prominent factors in affecting the intensity and FWHM of a diffraction peak, the present observations indicate that higher $O_2$ ratio used in the sputtering gas may have played an important role in improving the crystallinity of the *a*-axis-oriented ZnO thin films. Although it has been pointed out that, unless very reducing conditions are used, it is very difficult to change the oxygen vacancy concentration at temperatures below 1000 °C [4]. Thus, it is not obvious why by merely changing the $O_2$ ratio in the sputtering gas would lead to such noticeable effects in film microstructure. One possibility is that, since the oxygen atoms have higher electronegativity [23] and lower sputtering yield than argon atoms, therefore, they may recombine with electrons in the plasma more easily and result in lower ionic density in the plasma. The film, thus, grows under a lower sputtering rate but more oxidizing atmosphere and, as a consequence, more ordered manner, as indicated by the XRD results. In fact, one can also estimate the grain size, *D*, of the corresponding films by using the Scherrer's equation shown below [24]:

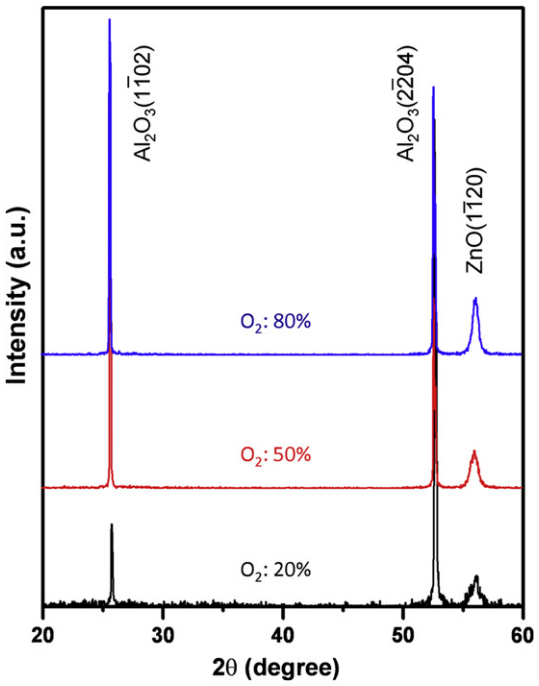


**Fig. 2.** XRD patterns of *a*-plane ZnO thin films deposited with various $O_2$ ratios.

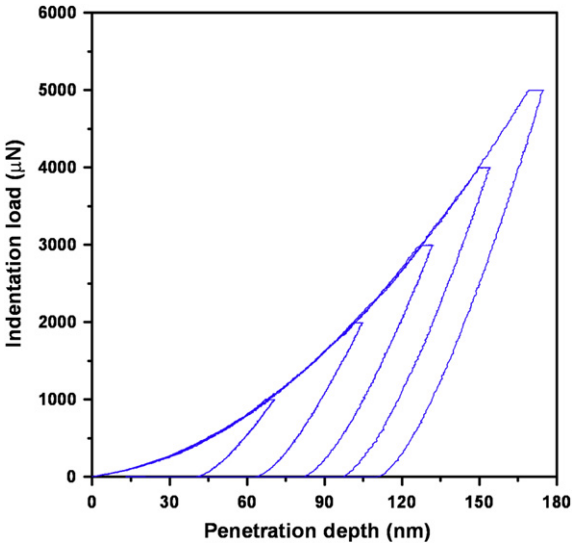


**Fig. 3.** Typical load–displacement curves with different peak loads from an indentation tests on *a*-plane ZnO thin films with the $O_2$ ratio of 80%.

$$D = \frac{0.9\lambda}{B\cos\theta}, \tag{4}$$

where $\lambda$, $B$ and $\theta$ are denoted as the X-ray wavelength, the FWHM of ZnO $(11\bar{2}0)$ -oriented peak and Bragg diffraction angle, respectively. The estimated grain sizes for the *a*-plane ZnO thin films with the $O_2$ ratio of 20%, 50% and 80% are 40, 72 and 86 nm, respectively, displayed as open circles shown in Fig. 3.

The typical cyclic nanoindentation curve obtained for the *a*-plane ZnO thin film deposited with an $O_2$ ratio of 80% is displayed in Fig. 4. It is noted that, in order to obtaining the properties of the epitaxial layer and avoiding the influences from the underlying substrate, the experiments were carried out with the maximum load and penetration depth being below about 5 mN and 160 nm, respectively. By using the analytic method developed by Oliver and Pharr [18], the hardness and Young's modulus of the *a*-plane ZnO thin films deposited with various $O_2$ ratios can be obtained. As shown in Fig. 3, the average values of hardness are 10.7, 9.2, 8.4 GPa for films deposited with the $O_2$ ratio of 20%, 50% and 80%,

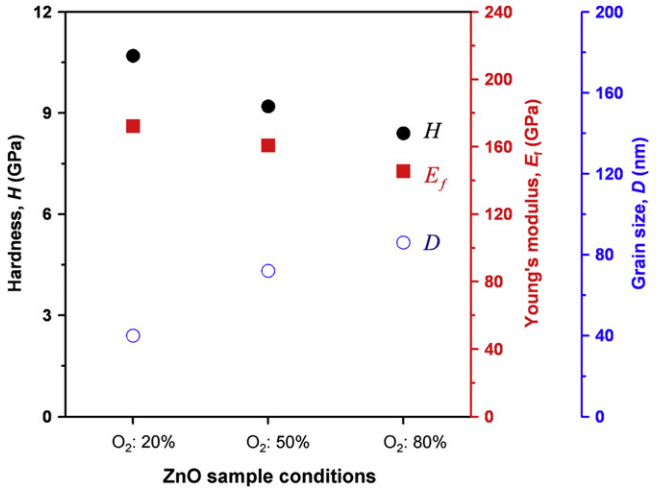


**Fig. 4.** Hardness, Young's modulus and grain size of *a*-plane ZnO thin films with different $O_2$ ratios.

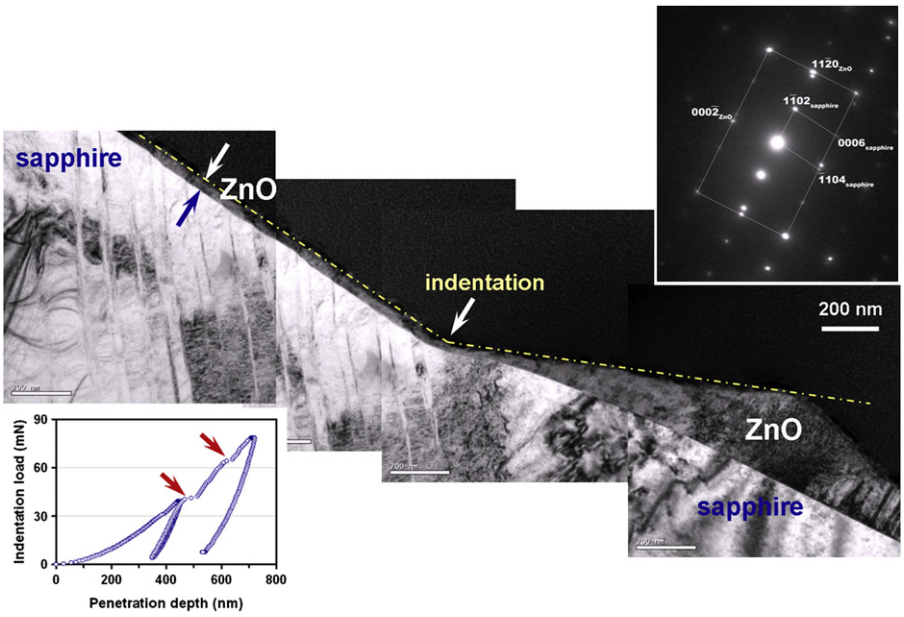


**Fig. 5.** Bright-field XTEM image of *a*-plane ZnO thin film deposited with the $O_2$ ratio of 80% subjected to an indentation load of 80 mN (In load–displacement figure, the red arrows are denoted as the multiple pop-ins). The inset showing the corresponding selected area electron diffraction pattern taken from the interface between ZnO epitaxial layer and substrate along sapphire $(11\bar{2}0)$ direction. (For interpretation of the references to colour in this figure legend, the reader is referred to the web version of this article.)

respectively. In addition, the average values of Young's modulus for the corresponding films are 172.4, 160.8, 145.5 GPa, respectively. It is evident from the results shown in Fig. 3 that both the hardness and Young's modulus of the obtained ZnO thin films decrease with increasing grain size resulted from increasing $O_2$ ratio in the sputtering gas mixture, which is also qualitatively consistent with what one would expect from the Hall–Petch effect [25]. We note that while the value of the hardness in the present case is considerably higher than the *a*-axis ZnO films grown by molecular beam epitaxy (MBE) (6.6 ± 1.2 GPa) and than that of the bulk layer (2 ± 0.2 GPa for *a*-axis and 4.8 ± 0.2 GPa for *c*-axis), the value of the Young's modulus here is much closer to bulk value (163 ± 6 GPa for *a*-axis and 143 ± 6 GPa for *c*-axis) than that of the MBE-derived films (318 ± 50 GPa) [7]. The values are also larger than those obtained for single crystal ZnO, in that the hardness and Young's modulus of 5.0 ± 0.1 and 111.2 ± 4.7 GPa are reported [26]. Although the increase of both the hardness and Young's modulus in MBE-derived films as compared to the bulk values has been attributed to the strain compensation arising from the pre-existent threading dislocations [7], it is not clear at present what causes the apparent discrepancies between the current results and that reported in Ref. [7]. However, the usage of different indenters might be one of the reasons responsible.

In order to identify the prevailing deformation mechanisms specific to the *a*-axis-oriented ZnO thin films subjected to the Berkovich nanoindentation, direct analyses on the microstructural characteristics in the vicinity of indented area are in order. A bright-field XTEM image of the *a*-plane ZnO thin film deposited with the 80% $O_2$ sputtering gas after indented with an indentation load of 80 mN is displayed in Fig. 5. Here, unlike that practiced to obtain the hardness and Young's modulus, the indentation load was intentionally increased to 80 mN to activate all the possible deformation mechanisms. We first discuss the selective area electron diffraction pattern shown in the upper inset of Fig. 5. It clearly demonstrates the $(1\bar{1}02)$ $Al_2O_3$//$(11\bar{2}0)$ ZnO epitaxial relationship between film and substrate. Next, we notice that there is no evidence of dislocation propagation-induced slip band observed within the film, which is consistent with the results reported by Coleman et al. [7] and had been attributed to strain accommodation provided by the pre-existing threading dislocations. It is even more surprising to observe that this effect has, in fact, resulted in localized deformation behavior. As is evident from Fig. 5, although due to the exceedingly large load applied there are apparent pile-ups at the edges of the indent (see also the inset SEM photograph in Fig. 1) and even the induced slip bands occurring in the substrate, the regions just beyond the pile-ups appear to remain relatively undeformed. As can be seen near the end of lower right area in Fig. 5, the threading dislocations remained straight, indicating not much deformation and associated dislocation interactions occurring there. Moreover, even with the extensive deformation-induced damage directly underneath the indent, there is no crack within the ZnO film or delamination at the film/substrate interface. Nevertheless, as mentioned above, plastic deformation confined to the region beneath the Berkovich indenter tip is evident in the substrate. Several narrow slip bands are clearly observed, which are inclined at an angle of ~57o with respect to the $(1\bar{1}02)$ surface, indicating that they are aligned on the {0001} planes. The corresponding load–displacement curve (the lower-left inset in Fig. 5) shows the multiple pop-ins in the loading, which are presumably associated with the onset of slip inside the sapphire substrate. The occurrence of multiple "pop-ins" has been linked to abrupt plastic flow generated by high dislocation nucleation and propagation rates [9,10,20,22], crack formation [12] or phase transformation [27]. Finally, the reverse discontinuities during unloading curve, the so-called "pop-out" event, commonly observed in silicon and has been attributed to pressure-induced phase transition [21,28] is not observed here. Therefore, in this case, neither phase transformation in the substrate nor through-thickness cracks in the *a*-plane ZnO thin films have been observed.

## 4. Conclusion

In summary, the structural features and mechanical responses of the *a*-plane ZnO thin films produced by using RF sputtering process at the various $O_2$/Ar ratios were investigated by XRD, nanoindentation, and XTEM techniques. The intensity of the ZnO-

$(11\bar{2}0)$ diffraction peak increases with increasing $O_2$ partial pressure while the peak FWHM shows the opposite dependence, both indicate the improved film crystallinity with the higher oxygen partial pressure. The average values of hardness and Young's modulus of the *a*-plane ZnO thin films are 10.7, 9.2, 8.4 GPa and 172.4, 160.8, 145.5 GPa for films obtained with $O_2$/Ar ratio of 20%, 50% and 80%, respectively. The XTEM observations revealed that, even at high indentation loading, the deformation of these *a*-axis-oriented ZnO thin films exhibits extremely localized behavior, namely the dislocations do not propagate beyond the pile-up regions near the edge of the Berkovich indenter. Despite of the occurrence of slip bands aligning on the {0001} planes of the sapphire substrate due to this high indentation load, there is no bending at the film/substrate interface or any phase transformation occurred in the substrate.

## Acknowledgments

This work was partially supported by the National Science Council of Taiwan, under Grant Nos.: NSC 97-2112-M-214-002-MY2, NSC99-2112-M-214-001 and NSC100-2221-E-214-024. JYJ is partially supported by the National Science Council and the MOE-ATU program operated at NCTU. Author likes to thank Dr. Y.-S. Lai and Dr. P.-F. Yang for their useful discussion and technical supports.

## References

[1] M. Law, L.E. Greene, J.C. Johnson, R. Saykally, P.D. Yang, Nat. Mater. 4 (2005) 455.
[2] P.F. Garcia, R.S. McLean, M.H. Reilly, Appl. Phys. Lett. 88 (2006) 123509.
[3] D.K. Hwang, M.S. Oh, J.H. Lim, S.J. Park, J. Phys. D: Appl. Phys. 40 (2007) R387.
[4] D.L. Hou, R.B. Zhao, Y.Y. Wei, C.M. Zhen, C.F. Pan, G.D. Tang, Curr. Appl. Phys. 10 (2010) 124.
[5] P. Misra, Y.J. Sun, O. Brandt, H.T. Grahn, J. Appl. Phys. 96 (2004) 7029.
[6] C.R. Gorla, W.E. Mayo, S. Liang, Y. Lu, J. Appl. Phys. 87 (2000) 3736.
[7] V.A. Coleman, J.E. Bradby, C. Jagadish, P. Munroe, Y.W. Heo, S.J. Pearton, D.P. Noron, M. Inoue, M. Yano, Appl. Phys. Lett. 86 (2005) 203105.
[8] L. Bao, Z.H. Xu, R. Li, X.D. Li, Nano Lett. 10 (2010) 255.
[9] T.H. Sung, J.C. Huang, J.H. Hsu, S.R. Jian, Appl. Phys. Lett. 97 (2010) 171904.
[10] S.R. Jian, G.J. Chen, T.C. Lin, Nanoscale Res. Lett. 5 (2010) 935.
[11] S.R. Jian, J.Y. Juang, N.C. Chen, Jason S.C. Jang, J.C. Huang, Y.S. Lai, Nanosci. Nanotechnol. Lett. 2 (2010) 315.
[12] C.Y. Yen, S.R. Jian, G.J. Chen, C.M. Lin, H.Y. Lee, W.C. Ke, Y.Y. Liao, P.F. Yang, C.T. Wang, Y.S. Lai, Jason S.C. Jang, J.Y. Juang, Appl. Surf. Sci. 257 (2011) 7900.
[13] P.F. Yang, H.C. Wen, S.R. Jian, Y.S. Lai, S. Wu, R.S. Chen, Microelectron. Reliab. 48 (2008) 389.
[14] S.R. Jian, I.J. Teng, P.F. Yang, Y.S. Lai, J.M. Lu, J.G. Chang, S.P. Ju, Nanoscale Res. Lett. 3 (2008) 186.
[15] Q.W. Li, J.M. Bian, J.C. Sun, H.W. Liang, C.W. Zou, Y.L. Sun, Y.M. Luo, Appl. Surf. Sci. 257 (2010) 1634.
[16] S.P. Wang, C.X. Shan, B. Yao, B.H. Li, J.Y. Zhang, D.X. Zhao, D.Z. Shen, X.W. Fan, Appl. Surf. Sci. 255 (2009) 4913.
[17] X. Li, B. Bhushan, Mater. Charact. 48 (2002) 11.
[18] W.C. Oliver, G.M. Pharr, J. Mater. Res. 7 (1992) 1564.
[19] I.N. Sneddon, Int. J. Eng. Sci. 3 (1965) 47.
[20] S.R. Jian, J.Y. Juang, Y.S. Lai, J. Appl. Phys. 103 (2008) 033503.
[21] S.R. Jian, G.J. Chen, J.Y. Juang, Curr. Opin. Solid State Mater. Sci. 14 (2010) 69.
[22] C.H. Chien, S.R. Jian, C.T. Wang, J.Y. Juang, J.C. Huang, Y.S. Lai, J. Phys. D: Appl. Phys. 40 (2007) 3985.
[23] T. Nagata, A. Ashida, N. Fujimura, T. Ito, J. Appl. Phys. 95 (2004) 3923.
[24] B.D. Cullity, S.R. Stock, Element of X-ray Diffraction, Prentice Hall, New Jersey, 2001, p. 170.
[25] S. Zhang, D. Sun, Y.Q. Fu, H.J. Du, Surf. Coat. Technol. 167 (2003) 113.
[26] S.O. Kucheyev, J.E. Bradby, J.S. Williams, C. Jagadish, M.V. Swain, Appl. Phys. Lett. 80 (2002) 956.
[27] D.J. Oliver, J.E. Bradby, J.S. Williams, M.V. Swain, P. Munroe, J. Appl. Phys. 101 (2007) 043524.
[28] S.R. Jian, Nanoscale Res. Lett. 3 (2008) 6.